

## 12. Satellite Orbit and Data Sampling Requirements

*William Rossow, NASA Goddard Institute for Space Studies*

Climate forcings and feedbacks vary over a wide range of time and space scales (cf., Peixoto and Oort, 1992). The operation of non-linear feedbacks can couple variations at widely separated time and space scales (e.g., Barnett, 1991) and cause climatological phenomena to be intermittent (Lorenz, 1990). Consequently, monitoring of global, decadal changes in climate requires global observations that cover the whole range of space-time scales and are continuous over several decades. The sampling of smaller space-time scales must have sufficient statistical accuracy to measure the small changes in the forcings and feedbacks anticipated in the next few decades (see Section 3 above), while continuity of measurements is crucial for unambiguous interpretation of climate change. Shorter records of monthly and regional (500-1000 km) measurements with similar accuracies can also provide valuable information about climate processes, when "natural experiments", such as large volcanic eruptions or El Ninos occur. In this section existing satellite datasets and climate model simulations are used to test the satellite orbits and sampling required to achieve accurate measurements of changes in forcings and feedbacks at monthly frequency and 1000 km (regional) scale.

### Orbit Selection - Coverage and Sampling Frequency

The geographic coverage and sampling frequency of satellite observations are principally determined by the orbit and are the leading criteria for orbit selection. Other important selection criteria are instrument spatial resolution, the pattern of coverage of Earth's surface, the range of solar illumination geometries encountered, payload mass and mission lifetime. The payload mass that can be orbited by a particular launch vehicle is larger for lower altitude orbits; larger launch vehicles cost more than smaller launch vehicles. The instrument mass and cost required to attain a particular spatial resolution are lower in lower altitude orbits. Satellite mission lifetime is strongly limited by atmospheric drag in low (< 400 km) altitude orbits and by radiation damage rates in high (> 1000 km) altitude orbits.

All of these issues have been studied thoroughly for previous satellite missions and have also been considered in selecting possible orbits for Climsat, but the focus here is on the two most important requirements for monitoring climate changes: complete global coverage and unbiased sampling of diurnal variations. The observing system proposed for Climsat that meets these requirements has the same set of instruments in two orbits: a near-polar sun-synchronous orbit and an inclined and precessing orbit (Fig. 12.1). Orbital altitudes in the range of 500-700 km allow for high enough spatial resolution with a small payload mass and for mission lifetimes  $\geq 5$  years.

In the atmosphere, diurnal variations are the shortest periodic variation with significant amplitude (cf., Peixoto and Oort, 1992). These variations also interact with the daily variation of solar illumination and the surface to alter several key climate forcings and feedbacks. Emphasis is therefore placed on proper sampling of diurnal

### Climsat Orbit Requirements

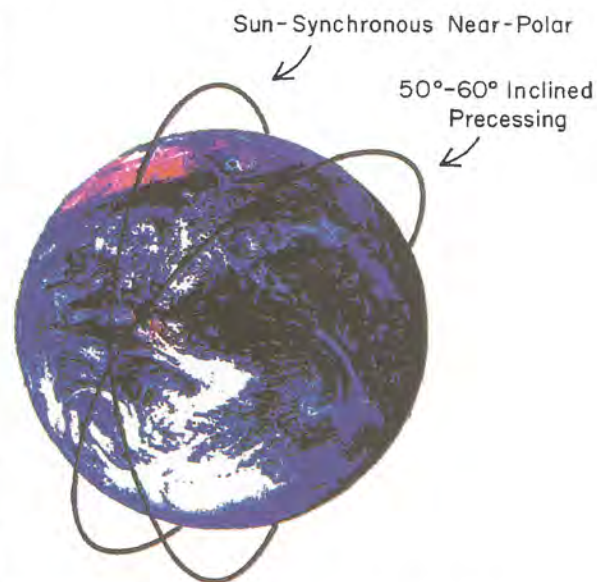


**Fig. 12.1.** Required satellite orbits for the Climsat observing system.

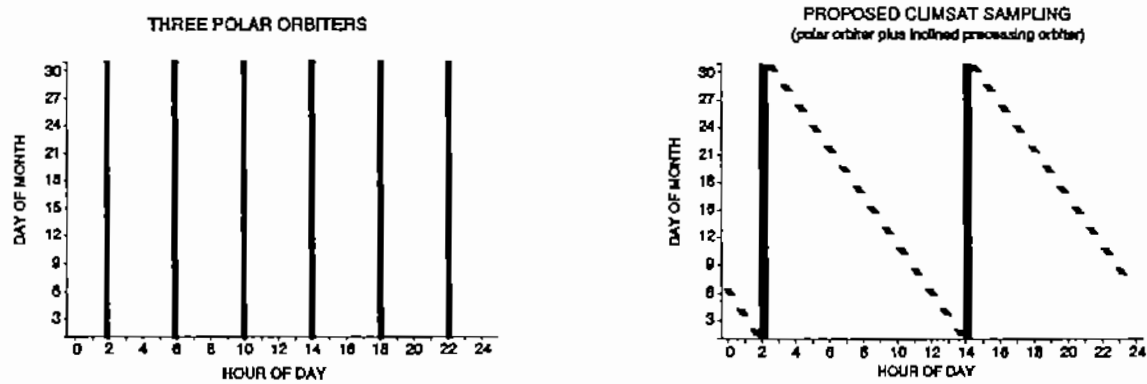


Fig. 12.2. Two alternative sampling strategies for adequate diurnal sampling.

variations, because it produces the strictest requirements. Proper diurnal sampling insures proper sampling of larger synoptic and planetary wave motions as well.

Global coverage and diurnal sampling cannot be satisfied by observations from one satellite (cf., Salby, 1982). A satellite in a polar orbit can view the whole Earth because of Earth's rotation, but the sampling frequency is only twice per day for orbital altitudes between 400-1000 km. The view from a satellite in an equatorial orbit is limited to low latitudes, but the sampling frequency can be more than 10 times per day. Geostationary orbits are special cases, where the view is restricted in both longitude and latitude, but the sampling frequency is limited only by instrument capability.

Figure 12.2 illustrates the sampling from two sets of orbits that provide global observations which adequately resolve diurnal variations. The simplest, direct method requires three sun-synchronous polar orbiting satellites with overflight times about four hours apart (Fig. 2, left panel), each providing two daily samples separated by 12 hours local time (Salby, 1982, 1988b, 1989). The major drawback of this approach for Climsat is that such polar orbits do not provide lower latitude coverage for the SAGE observations. SAGE, unlike most other instruments, must view the sun or moon at Earth's limb (see Section 8); this viewing geometry constrains observations to high latitudes from a polar orbit.

The observing scheme proposed for Climsat (Fig. 12.2, right panel) has only two satellites: one in an inclined orbit which precesses relative to the sun and one in a sun-synchronous polar orbit. The precessing orbit, inclined 50-60° to the equator, provides daily observations at two local times, separated by 12 hours, that vary slowly during the month (slanting lines). Observations from this orbit provide a statistical sample of diurnal variability at all latitudes where it is significant (McConnell and North, 1987; Shin and North, 1988; Bell *et al.*, 1990). The sun-synchronous orbit provides two daily observations over the whole globe at fixed diurnal phases, which allows for separation of diurnal variations from other oscillations with periods near one-half month (Harrison *et al.*, 1983). A similar sampling scheme was successfully used in the ERBE mission (Brooks *et al.*, 1986).

When observations are made in the nadir direction from this pair of orbits over one day, they cover the globe with an effective spacing of about 500-1000 km; Fig. 12.3 shows the orbits projected onto Earth's surface, called the ground tracks. The polar orbiter completes about 14 orbits per day with ground tracks that can be precisely repeated or their longitude can oscillate slightly over several days. The inclined orbiter also completes about 14 orbits per day, but the ground track precesses 5-6° of longitude per day so as to sample diurnal variations. This arrangement of orbits also permits solar occultations at all latitudes for SAGE (Fig. 12.4 shows the distribution of observations). Lunar occultations by SAGE III will increase the density of observations by about 50% over that shown in Fig. 12.4.

1 Day's Ground Tracks for Polar & Inclined Orbiter

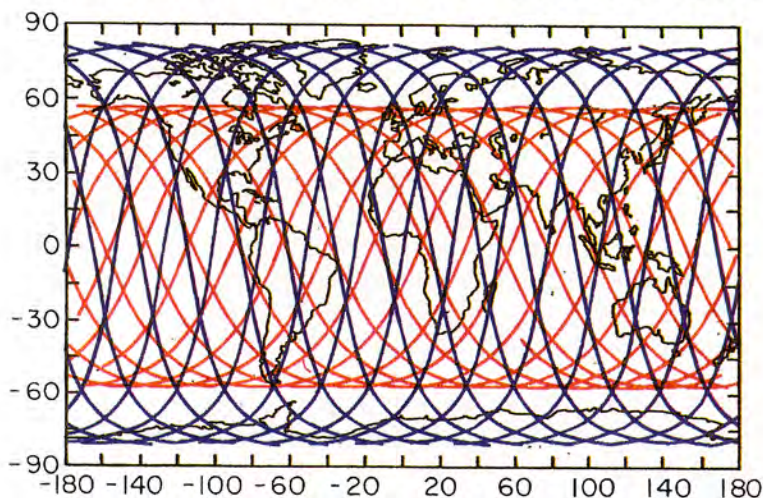


Fig. 12.3. One day's orbit ground tracks for polar (blue) and inclined (red) orbiters.

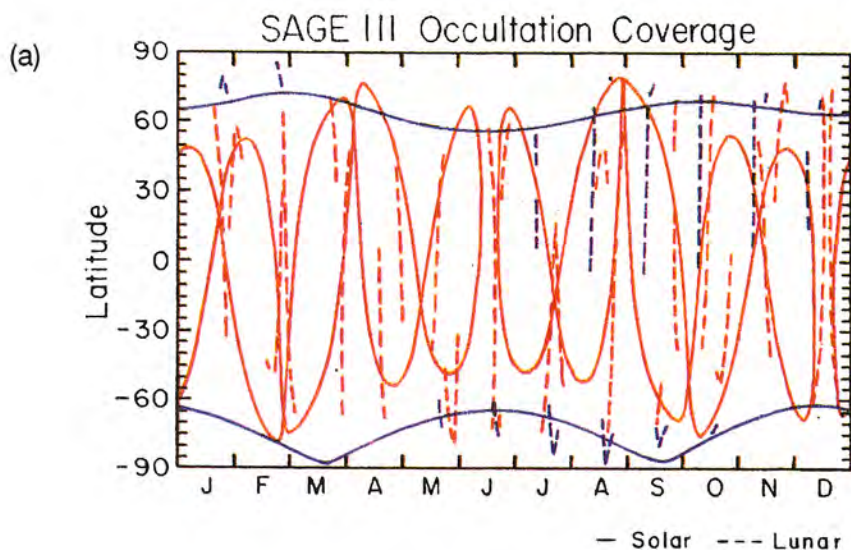
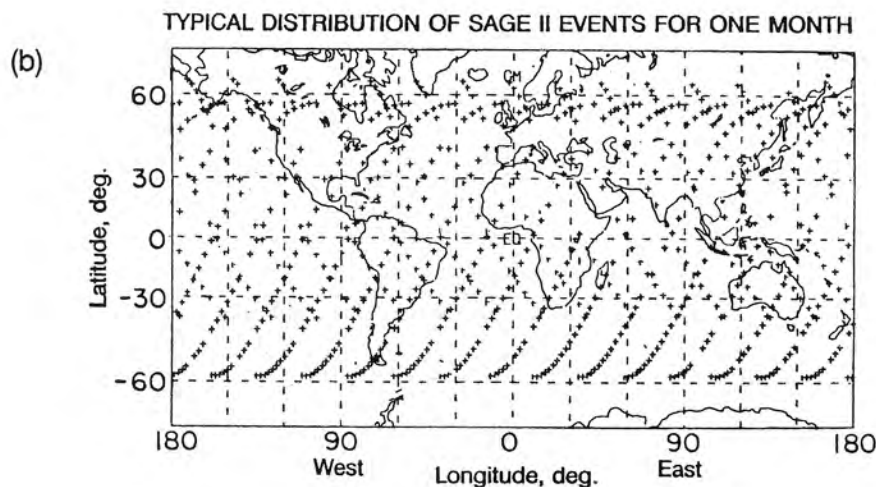


Fig. 12.4. (a) SAGE III solar and lunar occultation coverage over one year. Polar orbiter in blue and inclined in red. (b) typical SAGE sampling for one month from single satellite (inclined orbit, solar occultation). Lunar occultation increases density of observations about 50 percent; polar orbiter adds high latitude observations.



### Tests of Climsat Sampling

To test the Climsat observing strategy, real global observations and GCM calculations of several quantities are sampled using actual time records of the satellite ground tracks illustrated above. Samples are collected into global maps and averaged over time and space. Sampling errors are estimated from the differences between the monthly, regional mean values obtained from the sampled and original (taken to be "truth") datasets. The sampling test using real observations directly determines the accuracy of Climsat measurements of monthly, regional averages in the presence of realistic variations in time and space (cf., Section II). The sampling test using a GCM simulation of transient climate change allows a direct test of climate change detection, where the key problem is measuring the change in the presence of large natural variability (e.g., Oort, 1978 and Hansen and Lebedeff, 1987, used GCM simulations to test sampling, cf., Section I).

Ground tracks are from NOAA-9 (polar orbiter) and ERBS (inclined orbiter), giving positions every five seconds (about 30 km) over one month. The global observations are high resolution (30 km) measurements of cloud and surface properties every three hours for two Januarys and two Julys, obtained by the International Satellite Cloud Climatology Project (ISCCP) from weather satellite data (Rossow and Schiffer, 1991). Another dataset contains daily satellite measurements of humidity profiles at about 250 km spacing over the globe.

The climate change simulation is performed with the GISS GCM (Hansen *et al.*, 1983), which has  $8^\circ \times 10^\circ$  horizontal resolution and nine levels in the troposphere. The experiment simulates the transient climate changes produced by a linear increase of greenhouse gases (Scenario B, Hansen *et al.*, 1988); the climate change between 1958 and 2005 is used to test the Climsat sampling, since the global mean temperature change of  $0.8^\circ\text{C}$  is similar to the projected change from 1995 to 2015. Samples are collected from three hourly distributions of surface air temperature and vertical profiles of atmospheric temperature and specific humidity in the summers of 1958 and 2005. Sub-grid variations are represented by a bi-linear interpolation among the nearest model grid values to each sample point. In addition, random noise is added to each sample to represent both smaller scale variations and measurement errors: a Gaussian distribution is used, truncated at four standard deviations from the peak, with one standard deviation equal to  $2^\circ\text{C}$  for temperatures and equal to 30% of the local mean value for specific humidities at individual locations and altitudes.

Nadir observations are sampled at a spacing of about 30 km along the ground tracks. To simulate the same statistical weight obtained from multiple fields-of-view (FOV), an additional 6-9 samples around the nadir point are collected from the ISCCP dataset, but not from the GCM. Cross-track scanning is also tested on the GCM data by collecting about 200 points equally spaced on a line perpendicular to the satellite track at each nadir point. Since both the ISCCP and GCM datasets are composed of global maps at three-hour intervals, about 2200 nadir point samples are collected from each map.

In the tests using the ISCCP data, samples are taken directly from the population of individual satellite image pixels in the ISCCP dataset, so there is no "measurement error". Essentially, the sampling procedure isolates a subset of the ISCCP pixels (themselves, a sample of the original satellite measurements in FOVs about 5 km in size) that are concentrated at the locations and times defined by the orbit ground track time record. Monthly mean values obtained from the subset are compared to averages over the whole ISCCP population.

Sampling tests were conducted for surface temperature and reflectance, column abundances of ozone and water vapor, vertical profiles of temperature and specific humidity in the troposphere and stratosphere, and cloud properties. For brevity, only the results for cloud amount, surface air temperature and tropospheric humidity are shown. Cloud amount is highlighted because its very large natural variability in both space and time makes it one of the most difficult quantities to monitor

accurately. Surface temperature is tested because it has been the primary variable monitored for change and has the best understood sources of error. Water vapor is included both because it is highly variable (though not as variable as cloud cover) and difficult to measure, especially in the upper troposphere, so a large rms measurement error of 30% is included for each sample. The results show that the Climatsat sampling is more than adequate to monitor likely changes in these quantities.

**Sampling Clouds.** Cloud amount is determined by counting the fraction of satellite FOVs (pixels) in a map grid cell that are inferred to contain clouds. In other words, the cloud amount for a single pixel is either 0 or 100%. For ISCCP the original FOVs of about 5 km size have been sampled to a spacing of 30 km; however, this sampling preserves the statistics of the original radiance variations (S  ze and Rossow, 1991a,b). Cloud amount is determined for a map grid with a resolution of about 280 km and has been shown to be accurate to within 5–10%, even for the most difficult cases (Wielicki and Parker, 1992; Rossow and Garder, 1993).

The frequency distribution of cloud amount, as determined from the ISCCP three-hourly data, is bimodal (Rossow and Schiffer, 1991). The bimodal shape (Fig. 12.5, left panel) is nearly constant for data resolutions of 30–280 km, where only about 15–25% of the cases represent cloud cover variations at scales < 280 km (Rossow and Garder, 1993).

The bimodal distribution of cloud amounts means that the natural variability of cloud cover is very large and that sampling error can be very large, since the distribution can be thought of as a probability distribution for a single sample (Warren *et al.*, 1986, 1988). The standard deviation of the distribution in Fig. 12.5 is about 30–35% (Warren *et al.*, 1986, 1988 give values of about 40%), so that more than 1000 samples are required to reduce the sampling uncertainty below 1% (cf. Warren *et al.*, 1986, 1988). Thus, a test of the Climatsat sampling on cloud amount is a very strict test.

The accuracy of the monthly mean cloud amount determined from a nadir-viewing, non-scanning instrument in the Climatsat orbits is shown on the right side of Fig. 12.5 as the frequency distribution of the sampling errors in individual map grid cells. Reducing the map grid resolution from 2.5° to 10° narrows the range of errors (e.g., the standard deviation of the errors for January 1987 decreases from 7.8% to 3.3%) as does increasing the averaging time period from one month to one season (standard deviations for three month averages decrease to 4.7% for 2.5° map grid and to 2.1% for a 10° map grid). The sampling error for global, seasonal mean cloud amounts from the Climatsat orbits is less than 0.5%.

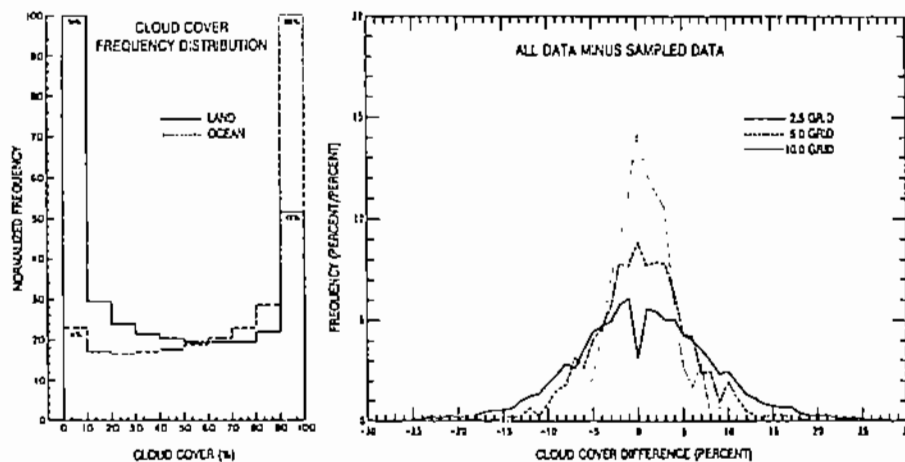
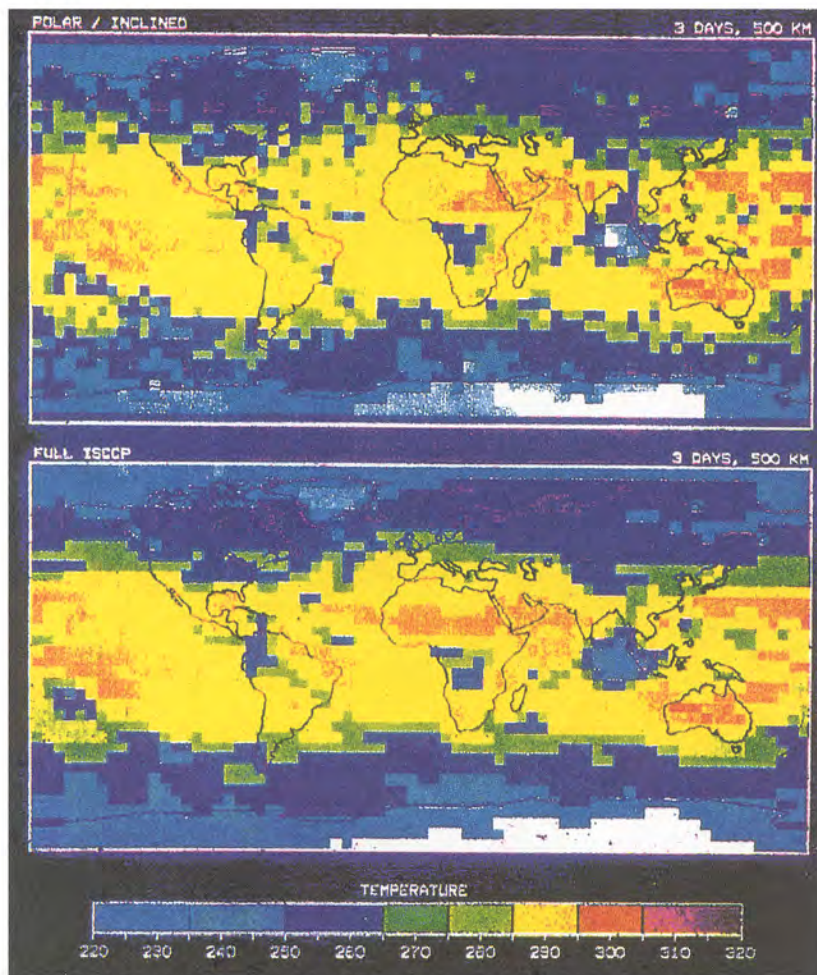


Fig. 12.5. Cloud cover frequency distribution for land and ocean and distribution of differences in monthly regional mean values produced by non-scanning sampling from Climatsat orbits.



**Fig. 12.6.** Cloud top temperatures obtained by non-scanning samples from Climatsat orbits over three days and by the 30 km sampling from the combination of geostationary and polar orbiting satellites used by ISCCP.

The magnitude of errors associated with diurnally biased sampling is assessed by comparing the cloud amount from the full ISCCP dataset to that determined only from the polar orbiter measurements (cf., Salby, 1988b). Bell *et al.* (1990) have considered the sampling bias from an inclined orbit similar to proposed for Climatsat (cf., Section II). Geographic and seasonal variations of both the amplitude and phase of diurnal changes of cloud amount produce a wide range of bias errors, from about -20% to +10%. Cloud variations in midlatitudes are predominately caused by synoptic scale motions, particularly in winter, so that the diurnal-bias error is generally < 5%; however, the predominance of convective scale cloudiness at low latitudes leads to a systematic bias of about 5 - 10% in tropical cloud amounts. Since climate changes may appear both as changes in total cloud amount or in the amplitude or phase of diurnal cloud variations, adequate diurnal sampling is critical for interpreting observed changes.

Cloud top temperatures are, generally, much less variable at smaller scales than cloud cover. Figure 12.6 compares the geographic distribution of cloud top temperatures, accumulated over a three day sampling period and averaged over 500 km, with the corresponding results from the full resolution (3-hour, 30 km) ISCCP dataset. Such a comparison is a more extreme sampling test because the accumulation period (3 days) is much shorter and the spatial resolution (500 km) higher than required by Climatsat objectives. The good agreement between the two datasets is readily apparent. The rms regional (10° resolution) error of seasonal means is < 1.5°C, which is about an order of magnitude smaller than the average geographic variations. The sampling error of the global, seasonal mean is < 0.3°C.

**Sampling Surface Temperature and Atmospheric Humidities.** A direct test of climate change detection is provided by using the orbital ground tracks to sample the GISS GCM simulations of changes in the summer climate between 1958 and 2005 forced by a linear increase of  $\text{CO}_2$  (Hansen *et al.*, 1988). The model global mean temperature increases by  $0.8^\circ\text{C}$ , the vertically integrated specific humidity increases by 7% and the upper tropospheric specific humidity increases by 17% over this time interval (Table 12.1). Three-hourly output is sampled using the same orbit ground tracks, the monthly or seasonal mean values are computed, and the difference between 2005 and 1958 are formed. These sampled climate changes are compared to those obtained using the full model outputs.

An estimate of the magnitude of variations at scales smaller than the GCM grid is provided by observed correlation distances and the scatter of surface temperatures and lower troposphere humidities (Fig. 12.7). The rawinsonde data are from the lower 48 contiguous US states and include all monthly means from January 1978 through December 1982 (D. Gaffen, Ph.D. thesis - see Gaffen, 1992; Gaffen *et al.*, 1991, 1992). Correlations of monthly anomalies of 850 mb temperature and dewpoint (a good predictor of surface to 500 mb precipitable water - cf., Gaffen *et al.*, 1991; Liu *et al.*, 1991) as a function of the separation distance indicate that significant variations of these quantities (dashed lines indicate the 95% significance levels) occur at scales  $\geq 300$  km. Thus, the dominant variations of these variables are associated with synoptic scale motions which are almost resolved by the GCM grid. Smaller scale variation has been represented by bi-linear interpolations to each sample point between the GCM values at the grid box centers with added random noise. This approach overestimates the amplitude of smaller scale variations but also underestimates the correlations.

Figure 12.8 shows the effects of sampling on estimation of changes in June mean surface air temperature. Figure 12.8a shows the model predicted changes between 1958 and 2005 and Fig. 12.8b shows differences measured with Climsat sampling. Figure 12.8c shows the differences between Figs. 12.8a and 12.8b (sampling error), while Fig. 12.8d shows the sampling errors with cross-track scanning. Table 12.1 shows that the sampling errors for a non-scanning instrument are about  $0.4^\circ\text{C}$  rms, which produces an error in the global mean temperature of only  $0.02^\circ\text{C}$ . Both of these are several times smaller than the predicted changes. Figure 12.9 shows the geographic distribution of predicted June humidity changes and sampling errors for the upper troposphere. These results (Table 12.1) show that the Climsat sampling errors for non-scanning instruments are about 12% rms and only -1% for the global mean, significantly smaller than the predicted changes.

Figure 12.10a shows the GCM-predicted changes in summer zonal mean specific humidities as a function of latitude and pressure and Fig. 12.10b shows the changes estimated with Climsat sampling. Figures 12.10c and 12.10d show the absolute sampling errors and the relative sampling

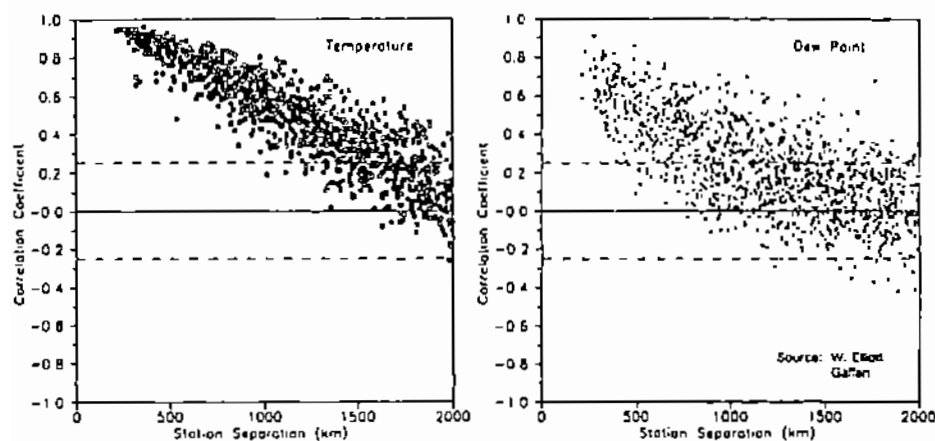


Fig. 12.7. Scatter diagrams of time record correlation coefficients for temperature and moisture against weather station separation distances.

**TABLE 12.1.** Changes between summer 1958 and 2005 in globally averaged surface air temperature, vertically integrated and upper tropospheric specific humidities as predicted by the GISS GCM compared with sampling errors using a nadir-viewing instrument in Climsat orbits with and without cross-track scanning.

	<u>Global Mean Values</u>		<u>Root Mean Square</u>	
		(%)		(%)
<b>Climate Change</b>				
Surface Air Temperature (°C)	0.80	—	2.06	—
Vertically Integrated Specific Humidity (g/kg)	0.15	7.19	0.25	9.47
Upper Troposphere Specific Humidity (g/kg)	—	17.23	—	47.18
<b>Sampling Error (No Scanning)</b>				
Surface Air Temperature (°C)	0.02	—	0.43	—
Vertically Integrated Specific Humidity (g/kg)	0.003	0.001	0.03	1.33
Upper Troposphere Specific Humidity (g/kg)	—	-0.96	—	11.74
<b>Sampling Error (With Scanning)</b>				
Surface Air Temperature (°C)	0.02	—	0.36	—
Upper Troposphere Specific Humidity (g/kg)	—	-0.05	—	11.33

errors expressed as a percentage of the "true" climate change in Fig. 12.10a. The model predicted changes are largest in the upper troposphere and lower stratosphere and are about an order of magnitude larger than the sampling errors (cf., Table 12.1).

The counter-intuitive result that sampling with scanning instruments does not produce significantly smaller errors than with non-scanning instruments (Figs. 12.8 and 12.9, Table 12.1) focuses attention on the difficulty of detecting climate changes. The main problem is that the natural variability of climate parameters, even on interannual time scales, may be larger than the climate changes predicted to occur over a few decades (Hansen *et al.*, 1988; Manabe *et al.*, 1990; Lorenz, 1990; Karl *et al.*, 1991). Some of the interannual variability in datasets is, in fact, residual error caused by sampling of synoptic variations of the atmosphere and surface. Thus, the limit on measuring climate changes accurately is determined by the magnitude of these natural variations, which can be considered the intrinsic "noise". That this is the case with the sampling errors shown in Figs. 12.8 and 12.9 and Table 12.1 is revealed by three facts.

First, the spatial patterns of the climate changes, shown in Figs. 12.8a and 12.9a, are similar in character to the pattern of differences between any two Junes in the GCM control run (no climate change forcing). In a typical case, the rms regional differences in surface air temperature are about 3.2°C and in upper tropospheric humidity are about 37%, very similar to the rms regional differences in the climate change experiment (Table 12.1). The global mean differences are, however, much smaller in the control run comparison (e.g., 0.2°C for surface air temperature and 1-2% for upper

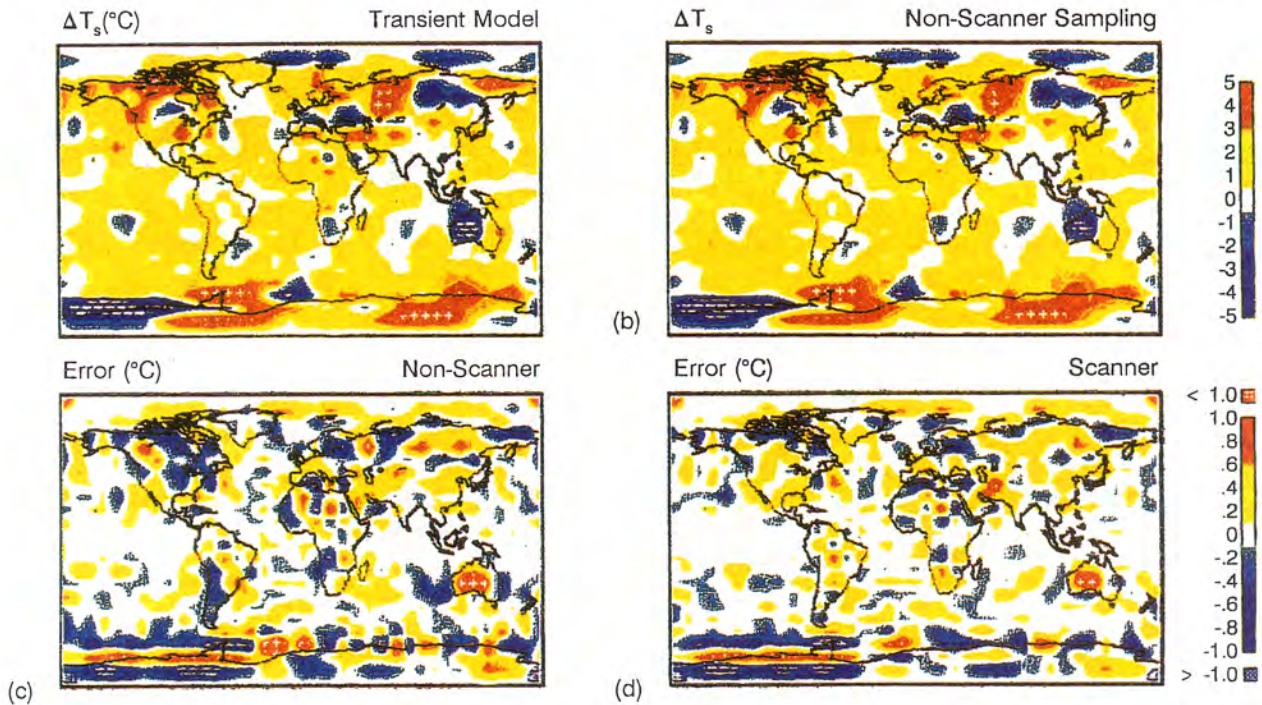


**Fig. 12.8.** Model-predicted changes (a) in monthly mean surface air temperature [(June 2005) – (June 1958)] and measured changes (b) with Climsat non-scanning sampling. Errors are shown as differences of (a) and (b) in (c). Differences produced by scanning sampling are shown in (d).

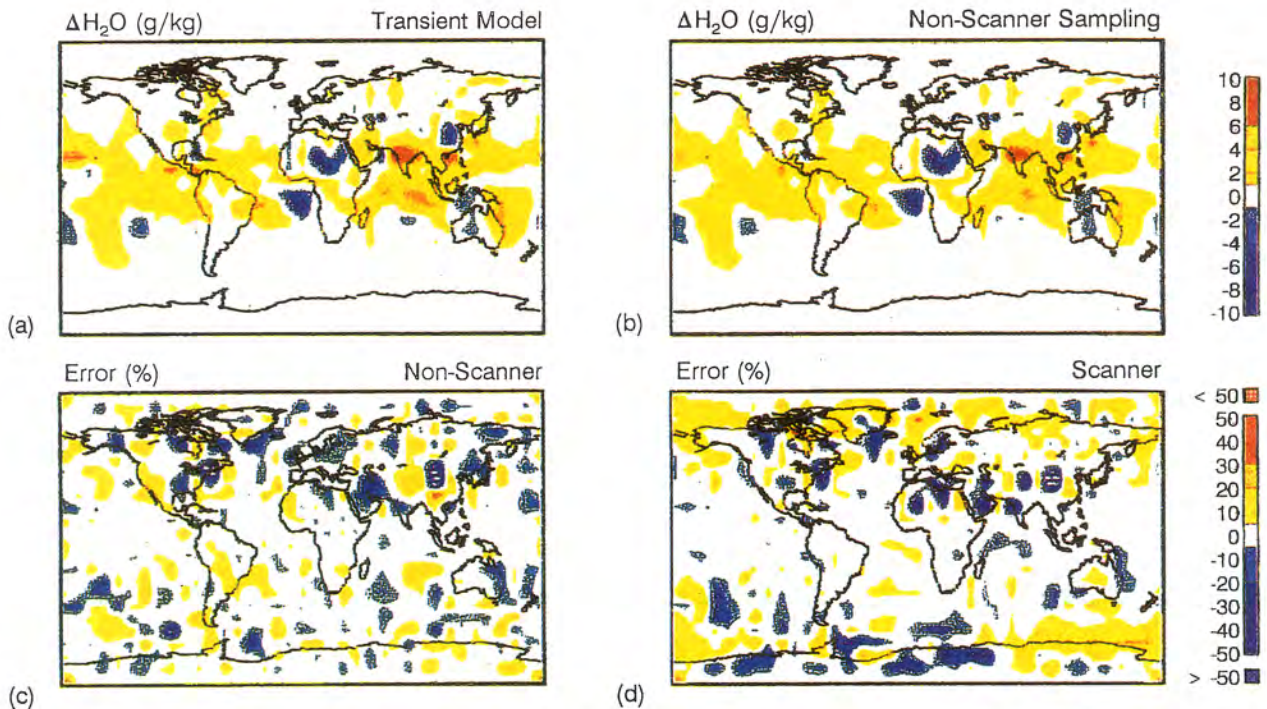


**Fig. 12.9.** Model-predicted changes (a) in specific humidity (g/kg) in the upper troposphere and measured changes (b) with Climsat non-scanning sampling. Errors are shown (in percent) for non-scanning sampling (c) and scanning sampling (d).

tropospheric humidity) than in the climate change comparison. Thus, the regional variability shown in Figs. 12.8a and 12.9a is predominately the consequence of different realizations of synoptic variations in any two months, rather than climate change. Moreover, changes in this regional variability between two months appear as differences in the global, monthly mean values of any parameter; in other words, this regional "noise" does not completely cancel in the global mean. Consequently, the global mean surface air temperature and upper tropospheric humidity changes are uncertain by at least  $0.2^{\circ}\text{C}$  and 1-2%, respectively, just because of natural variability.

Second, the sampling errors, shown in Figs. 12.8b and 12.9b, are proportional to the changes in Figs. 12.8a and 12.9a. This results from the fact that a one month time record of synoptic variability at one location actually represents only about 10-15 independent samples because the synoptic changes are correlated on time scales of a few days. Thus, for example, a single large storm event in a particular month will both increase the difference between monthly mean values and be more likely to increase the error in a sampled dataset because the storm is a "singular" event with low probability. This effect also explains why the natural variability in surface air temperature is a larger fraction of the climate change (about 25% of the global mean) than for upper tropospheric humidity (about 5% of the global mean), since the larger surface temperature variations occur at midlatitudes with longer correlation times (fewer samples) than the humidity variations which occur in the tropics with shorter correlation times (more samples).

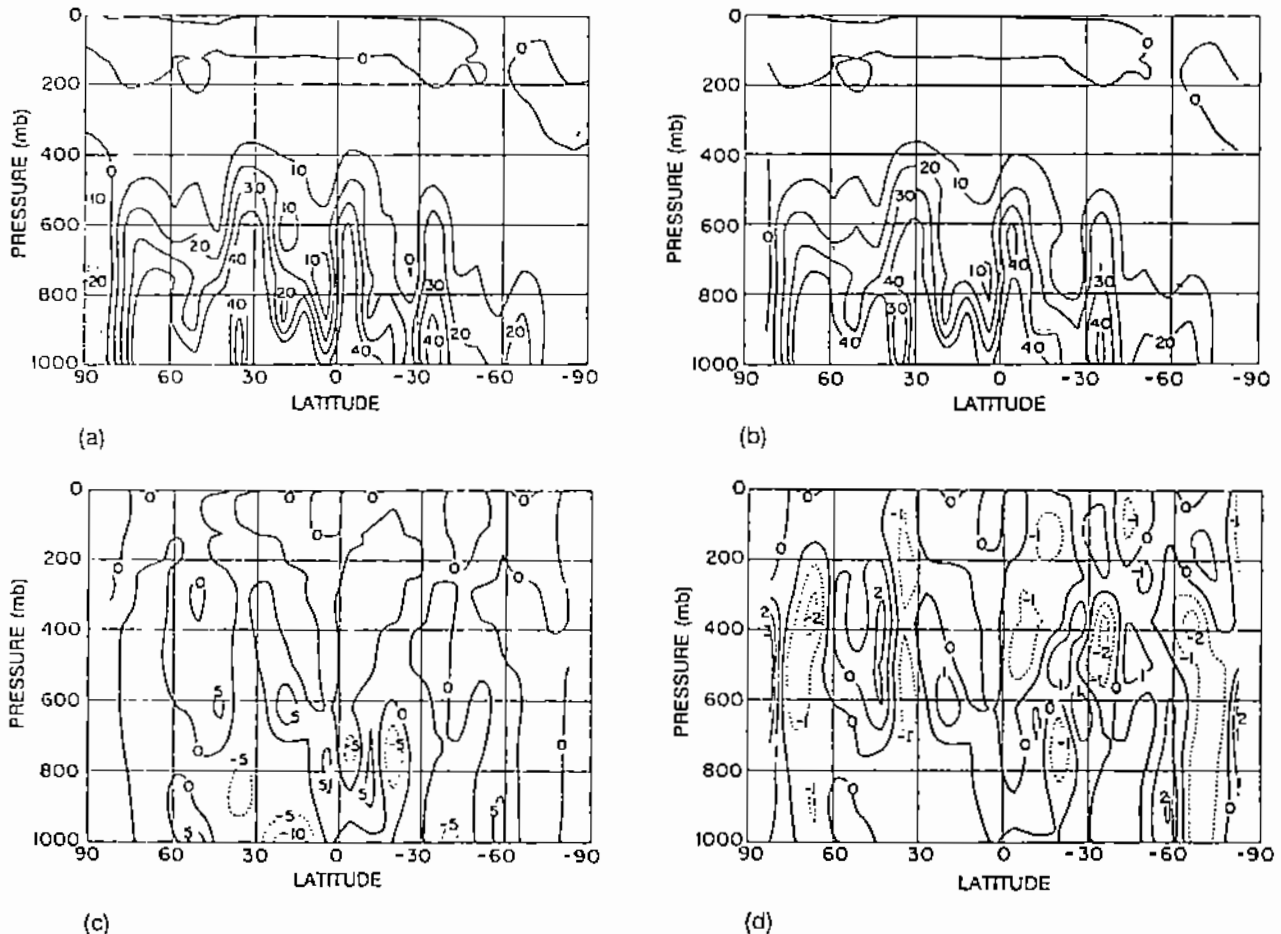


Fig. 12.10. Model-predicted zonal mean changes in specific humidity (a) the changes measured with Climsat non-scanning sampling (b) Absolute (c) and relative (d) differences are displayed in percent.

**TABLE 12.2.** Summary of all sampling tests. Regional averages are from a 10° map grid.

	Global Monthly <u>Average</u>	Global Seasonal <u>Average</u>	Regional Monthly <u>Average (rms)</u>
Surface temperature (°C)	< 0.2	< 0.1	< 0.5
Specific humidity errors (%) (vertical integrated) (upper troposphere)	< 0.1 < 2.0	< 0.1 < 1.0	< 2.0 < 12.0
Ozone column abundance (%)	< 0.03	< 0.02	< 2.0
Cloud top temperature (°C)	< 0.5	< 0.3	< 1.5
Cloud amount (%)	< 0.7	< 0.4	< 3.0

Third, the space-time distribution of the sampling from scanning instruments is different from that of non-scanning instruments, particularly at higher latitudes. The different distributions of the two sampling patterns interact with synoptic variations to produce about the same rms sampling errors but also cause differences in the measured global, monthly mean values of surface air temperature and upper tropospheric humidity that are as large as the differences between two months in the control run. In other words, these two sampling patterns can be considered as two different realizations of the natural variability, producing similar uncertainties in measured quantities. Thus, the much larger number of measurements made with the scanning instrument does not significantly reduce the sampling error which is already dominated by natural variability for the smaller non-scanning dataset.

These sampling studies confirm that the largest source of uncertainty in measuring climate change is limited sampling of natural (synoptic) variability, as long as the observing system provides complete and uniform global coverage and unbiased time sampling. (Even though the GCM tests assumed very large random measurement errors, the sample population for one month of data, even for non-scanning instruments, is so large as to nearly eliminate this source of uncertainty.) Since synoptic variations are correlated on time scales of a few days, the number of independent samples of these variations that can be obtained in one month (during which the forcing can be considered constant) is so small that the uncertainty in mean values remains much larger than predicted climate changes. Likewise, uncertainties in global mean values are not reduced by increasing the spatial resolution of observations because the synoptic variations are also correlated on large spatial scales (cf., Fig. 12.7), which places an intrinsic limit on the number of independent samples that can be obtained. These correlations explain why the non-scanning sampling from the Climatsat orbits is as good as the scanning sampling. Moreover, even if an observing system provides uniform space-time sampling, ordinary problems in operating instruments and computer systems cause data losses that produce gaps in spatial and temporal coverage that exaggerate the contribution of the intrinsic noise. Thus, the only way to reduce this source of sampling error enough to measure the predicted decadal climate changes is to make comparisons between observations averaged over at least 3-5 years in each of two decades.

Table 12.2 summarizes the results of the sampling studies using both data and GCM simulations by reporting the largest differences as upper limits on sampling errors. Comparison of these sampling errors with the accuracy requirements in Section 3 shows that Climatsat will generally be able to monitor plausible decadal changes of the forcings and feedbacks which it addresses (see also Section 7 and Table 7.4).